C3TM: CEI CCD charge transfer model for radiation damage analysis and testing

Conference or Workshop Item

C3TM: CEI CCD Charge Transfer Model for radiation damage analysis and testing

Jesper Skottfelt, David J. Hall, Ben Dryer, Ross Burgon, and Andrew Holland

Centre for Electronic Imaging, School of Physical Sciences, The Open University, Milton Keynes MK7 6AA, UK

ABSTRACT

Radiation induced defects in the silicon lattice of Charge Couple Devices (CCDs) are able to trap electrons during read out and thus create a smearing effect that is detrimental to the scientific data. To further our understanding of the positions and properties of individual radiation-induced traps and how they affect space-borne CCD performance, we have created the Centre for Electronic Imaging (CEI) CCD Charge Transfer Model (C3TM). This model simulates the physical processes taking place when transferring signal through a radiation damaged CCD. C3TM is a Monte Carlo model based on Shockley-Read-Hall theory, and it mimics the physical properties in the CCD as closely as possible. It runs on a sub-electrode level taking device specific charge density simulations made with professional TCAD software as direct input. Each trap can be specified with 3D positional information, emission time constant and other physical properties. The model is therefore also able to simulate multi-level clocking and other complex clocking schemes, such as trap pumping.

Keywords: CCD, radiation damage, simulations

1. INTRODUCTION

The radiation environment outside the Earths magnetosphere is an issue for most space-based detectors. Highly energetic particles from the Sun can damage Charge-Coupled Devices (CCDs) by creating defects in their silicon lattice. These defects are able to trap electrons during the read out of the CCD and thus create a smearing effect that is detrimental to the scientific data. As the demand for higher photometric and spatial precision in space-based imaging data keeps increasing, a better understanding of the effects of radiation induced defects are needed.

For that purpose we have created the Centre for Electronic Imaging (CEI) CCD Charge Transfer Model (C3TM) to simulate the physical processes taking place when transferring signal through a radiation damaged CCD. The model was described in some detail in Ref. 1, where it was known as OUMC, and it builds upon the heritage of a previous model iteration.[2–5]

C3TM is a is a Monte Carlo model based on Shockley-Read-Hall theory,[6,7] and mimics the physical properties in the CCD as closely as possible. To avoid making any analytical assumptions about the size and density of the charge cloud, the model takes device specific simulations of electron density as a direct input. The electron density simulations are made with the professional TCAD semiconductor device simulation software suite SILVACO[8] that requires detailed information about the device, such at electrode layout, doping profiles, etc. C3TM runs on a sub-electrode level and each trap can be specified with emission time constant, emission and capture cross sections, and three-dimensional positional information. The model is therefore also able to simulate multi-level clocking and other complex clocking schemes, such as trap pumping,[9–13] and its relation to charge loss.[14]

While the initial purpose of C3TM is to deliver input to the radiation damage correction efforts for the VISual instrument[15] on ESAs Euclid mission,[16] the code has been made such that it can be easily be adapted to detectors for other instruments. This means that the code could be beneficial for other current or future space missions.

Further author information: (Send correspondence to J.S.)
J.S.: E-mail: jesper.skottfelt@open.ac.uk, Telephone: +44 (0)1908 652 698

C3TM has already produced a number of results that has been able to further the knowledge on radiation induced defects in CCDs, and has given input to the in-orbit calibration routines for VIS, and to the properties of the CCD273 devices used for the VIS. Some of these results, and a couple of new ones, are described in the following.

2. MODELLING CHARGE CAPTURE AND EMISSION

2.1 Shockley-Read-Hall Theory

In Shockley-Read-Hall theory the capture and emission of an electron by a single trap is described as a decay process and can thus be modelled using two exponential time constants; the capture time constant

$$\tau_c = \frac{1}{\sigma_c n v_{th}} \tag{1}$$

and the emission time constant

$$\tau_e = \frac{1}{X \chi \sigma_e N_c v_{th}} \exp\left(\frac{E}{kT}\right). \tag{2}$$

Here σ_c and σ_e is the capture and emission cross-section, respectively, n is the electron concentration, v_{th} is the thermal velocity

$$v_{th} = \sqrt{\frac{3kT}{m^*_{ce}}} \tag{3}$$

N_c is the density of states in the conduction band

$$N_c = 2\left(\frac{2\pi m^*_{de} kT}{h^2}\right)^{3/2}, \tag{4}$$

and E is the energy level of the trap below the conduction band. m^*_{ce} and m^*_{de} are the electron masses used for conductivity and density of states calculations, respectively. X is the entropy factor that is associated with the entropy change for electron emission and χ is a factor added to allow for any field enhanced emission that can affect the trap emission time as well as dark current generation.[17] The probability of a capture or emission of an electron over a given time t can be calculated as

$$P_x = 1 - \exp\left(\frac{-t}{\tau_x}\right), \tag{5}$$

where x can be substituted with c or e for capture and emission, respectively.

However, if a trap has an emission time constant that is similar to (or shorter than) the phase time t (or t_{ph}), i.e. the time the charge stays in the phase, then it is possible that that trap can capture and release an electron multiple times. As Eq. 5 only takes a single capture or emission into account, it is advantageous to define the combined probability of capture/emission of an electron by an empty/occupied trap after a time t given both the capture and emission constants. Following the calculations made in Ref. 18, 19, the probability of a capture by an empty trap be expressed as

$$P_c = \frac{r_c}{r_{tot}}\left[1 - \exp(-r_{tot} t)\right] \tag{6}$$

and the probability of an emission by an occupied trap as

$$P_e = \frac{r_e}{r_{tot}}\left[1 - \exp(-r_{tot} t)\right], \tag{7}$$

where $r_x = \frac{1}{\tau_x}$ and $r_{tot} = r_c + r_e$.

2.2 Charge capture

The main issue when calculating the capture time constant τ_c for a specific trap, is the electron concentration n, as this depends on the density distribution of the electron packet within the pixel. This is highly dependant on pixel architecture and the nature and concentration of the dopants used in the manufacture process, and a precise analytical description of the charge density distribution n is therefore near impossible to obtain.

A number of different methods to solve this problem has been used by other charge transfer models,[19–22] however, common for these methods is that the real physical solution is being fitted with an analytical function, which will introduce some bias and which will only be suitable under certain operating conditions.

C3TM uses charge density simulations as a direct input, in order to get as close to the actual physical properties as possible. The charge density simulations are made with Silvaco ATLAS semiconductor device simulation software.[8] The ATLAS software can take a full 3D model of a pixel or register element of a CCD as input along with doping profiles, the temperature of the device and the voltages applied to the different phases of the CCD. This means that charge distribution in the device can be modelled under the exact operating conditions that is requested, and that the simulation can be redone if the operating conditions change. This includes the possibility for modelling the charge distribution when multi-level clocking etc. is applied.

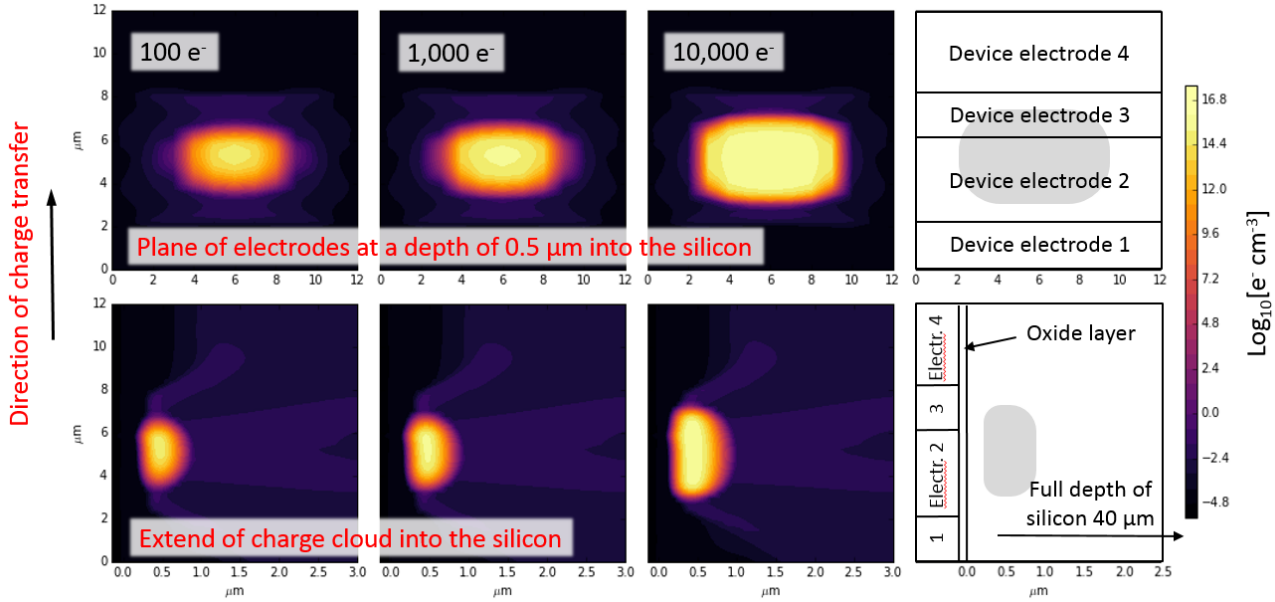

Figure 1. 2D cuts from 3D Silvaco ATLAS simulations of charge densities at different signal levels. The unit of the colorbar is $\log_{10}$[electrons/cm^3]. *Upper row*: The charge cloud at the plane of the electrodes, with the electrodes aligned with the x-axis and at a depth into the pixel of 0.5 µm. The plots shows the full 12x12 µm pixel. *Lower row:* The extend of the charge cloud into the pixel along the x-axis. The y-axis is the same as for the upper row, while the x-axis is only 3 µm. Figure from Ref. 1.

As the charge density changes with changing signal levels, the charge density simulations has to be done at a range of signal levels, from a single electron to Full Well Capacity. An example of charge clouds at different signal levels is given in Fig. 1, where the Euclid VIS CCD273 pixel has been simulated. For a single trap the charge density also changes with each single phase step, so τ_c needs to be calculated for each phase step and for all the signal levels given the 3D position of the trap in the pixel. In principle this means that Silvaco simulations of each phase step needs to be made, however, if two or more phase steps are adequately symmetric, i.e. that the shape of the potential is only flipped or displaced in one direction, C3TM is able to perform that change in order to decrease the number of Silvaco simulations needed.

Using a phase time $t_{ph} = 1\,\text{ms}$, the probability of capture P_c has been calculated from Eq. 5 and plotted in Fig. 2 to give an example of how P_c changes with signal level, position in the pixel, and over the different phase

steps. This shows that there is many orders of magnitude difference in the capture probability depending on the position of the trap in pixel and the signal level. To save time computational time, a maximum τ_c parameter can be set in C3TM, such that traps that have no τ_c values below that parameter, for any phase step or signal level, will be omitted completely from the simulations.

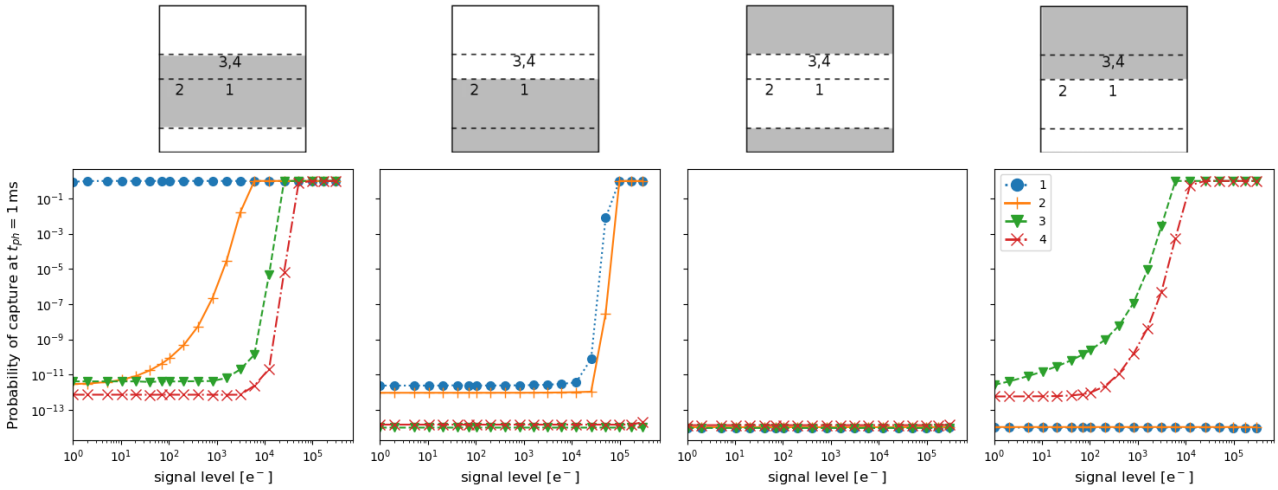

Figure 2. Calculated capture probabilities P_c for four traps at different positions. In each of the four columns, the charge has been shifted a single phase to simulate the readout of the CCD. *Upper row:* The panels outline the positions of the four phases. The phases containing the charge are marked in grey, and the first column is thus similar to the situation in Fig. 1. The numbers indicate the positions of four traps in the plane of the electrodes. Trap 1-3 is at a depth of 0.5 µm into the silicon, and trap 4 is at a depth of 0.75 µm. *Lower row:* The calculated P_c for the four traps using the trap positions and phases as shown in the panel above.

2.3 Charge emission

Until recently it was believed that traps of a certain species, defined by the energy level E, had very well defined emission time constants depending on the temperature, as shown in Fig. 3 where the "well-known" species and their appertaining emission time constants are plotted as a function of temperature. The plot also includes three species which are believed to be intrinsic in the CCDs coming from Phosphorus and Boron, which are used as dopants in the CCD manufacturing process, mixed with Carbon and Oxygen impurities that are naturally occurring in the silicon wafers.[23]

However, recent research using the trap pumping method has shown that emission time constants are not necessarily well-defined, but are better described as a broad distribution of τ_e values.[24,25] Recent studies where the CCD has been irradiated and kept at cryogenic temperatures while testing, has shown the existence of a continuum of τ_e values.[26]

C3TM has therefore been designed such that the emission time constants can either be assigned directly to the single traps using an input file, or they can be randomly assigned using a capture cross section σ_c, an energy level E and a spread on the energy level, for each of the species that needs to be included in the simulations. This means that a continuum can be created by defining a large enough spread on E.

It is also important to determine which charge packet an emitted electron will join. As an electron will always move towards higher potential, it is the potential structure in the pixel that determines in which direction the electron will go. In many cases the potential structure can be estimated using symmetry considerations, especially when a two-level clocking scheme is used and the phases have the same width. In more complex situations, however, it can be useful to extract the potential model from the Silvaco simulations. This is the case for the Euclid CCD273, which have phases of varying width and utilises multi-level clocking.

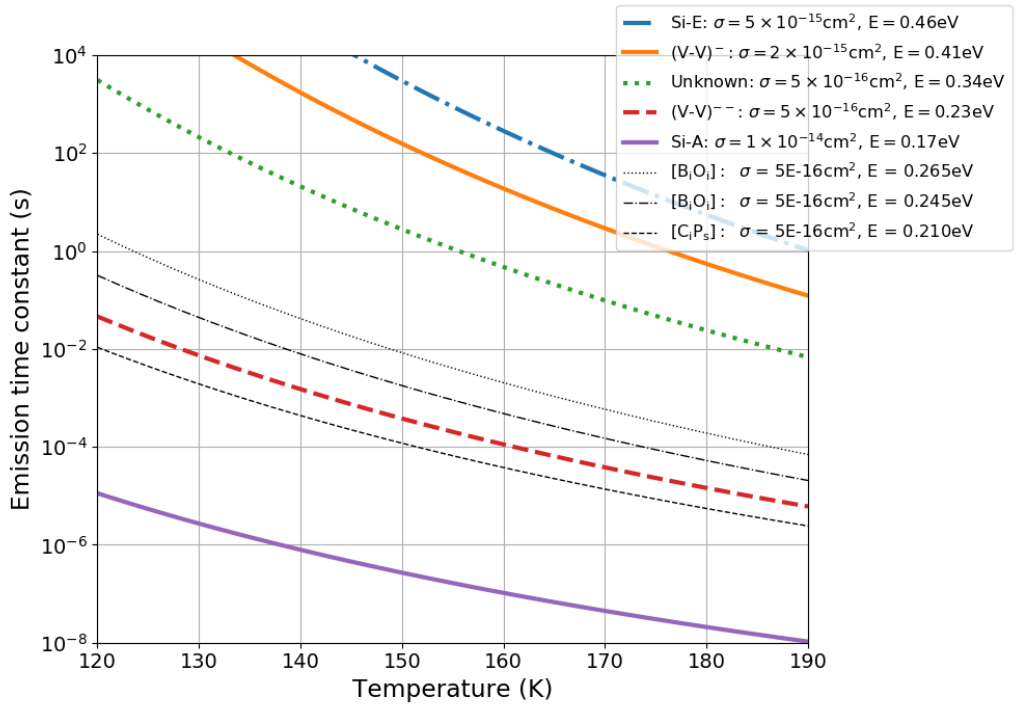

Figure 3. Emission time constants of different well-known defects in n-channel CCDs as a function of temperature. Also plotted are three species that is believed to be intrinsic in the CCD, due to the naturally occuring impurities in the silicon and the dopants used in the manufactoring process.[23]

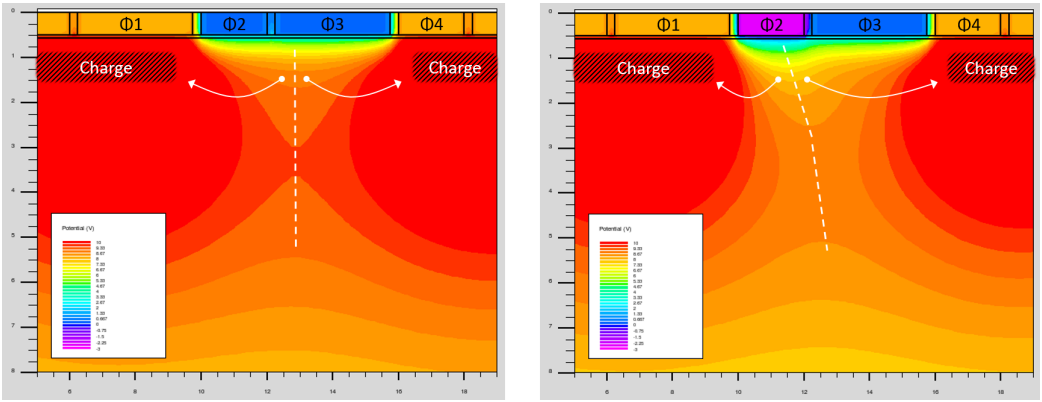

Figure 4. Silvaco simulations of the potential structure of the CCD273 pixel using two different voltage configurations; *(left)* Normal two-level clocking with phases 2 and 3 at 0V, and *(right)* tri-level clocking where phase 2 is at -3V and phase 3 is a 0V. Common for the two configurations is that phase 1 and 4 is at 8V. The upper limit of 10V is set to be able to see the contours of the potential well and the units on the axes are µm. The positions of the charge clouds and arrows showing the direction of the emitted electrons have been added to the plots. Figure from Ref. 1.

Figure 4 shows the potential structure extracted from Silvaco simulations of two different voltage configurations for the CCD273 pixel. In the left panel a two-level clocking scheme is used, such that phases 1 and 4 are biased at 8V and phases 2 and 3 is at 0V. This means that the point of the lowest potential in the x-direction is located midway between the end of phase 1 and the start of phase 4, or ∼3 µm from the rightmost edge of phase 1. Because of the 4-2-4-2 µm structure of the pixel, the lowest potential is therefore not between phase 2 and 3, but ∼1 µm into phase 3. An electron released from a trap at the leftmost fourth of phase 3 would therefore join

the charge packet in phase 1, and not the charge packet in phase 4 as it would if the phases had been the same width.

The right panel of Fig. 4 shows an example of tri-level clocking. Here phases 1 and 4 are still biased at 8V and phase 3 at 0V, but phase 2 has been set to -3V. The change of bias moves the point of the lowest potential some fraction of a phase width into phase 2, depending on the distance to the electrode. This means that electrons released from all traps in phase 3 and traps in the rightmost part of phase 2 will join the charge packet in phase 4. This information can be included in C3TM to improve the precision of the charge transfer simulations, especially in the more complicated cases.

2.4 Definition of pixels, traps and input arrays

For C3TM to work, a parameter file needs to be updated with information about the device, such as array and overscan sizes, pixel and phase dimensions, clocking schemes and phase times etc. It should be noted that much of this information can be changed while running C3TM, such that multiple runs with different parameters can be made in one go.

C3TM is a fully 3-dimensional model, so all trap positions needs to be defined with their x, y position in the pixel array, the electrode number the trap is under, the x, y, z position of the trap in the pixel, and the τ_e value. For most purposes, however, C3TM can randomly distribute traps in the array using a trap density for each species, given as traps pr. cm^3, and the energy level and energy level spread as described in the previous section. This will generate the needed information in an easy way. It is possible to store all trap information in a data file, such that it can be reloaded for another simulation. This can be done to make sure that the traps considered are the same, or the file can be edited to see what happens if particular parameters are changed directly.

The input array, or input scene, can either be generated by C3TM or it can be loaded from an existing array, for instance from a FITS file.[27] Several functions exists to easily generate flatfields, charge block or other shapes that are useful for the simulations, all at the signal level that is needed. The option to include existing data means that C3TM can also work on real data, or simulated images of stars and galaxies.

The output array can either be analysed directly or be stored in a FITS file. The FITS header will then contain all of the parameters that defines the particular simulation. It is also possible to store all the trap parameters in the FITS file as a FITS table.

3. RESULTS FROM C3TM

C3TM has shown to be very versatile and has already been used for a number of different studies. These have delivered a number of results that has been able to further the knowledge on radiation induced effects in CCDs and has given vital input to the in-orbit calibration routines for VIS. In this section we will shortly summaries some of these results.

3.1 Trap pumping dipole maps

As C3TM runs on a sub-electrode level it can be used to simulated the process of trap pumping. Trap pumping is a method where charge is clocked back and forth between the pixels such that each trap creates a dipole for which the intensity depends on how close the emission time constant is to the clocking time (see also Ref. 23). This means that information about the emission time constant, energy level, capture and emission cross sections, sub-pixel and even sub-phase positions for the single traps can be extracted and a much better constraint on the trap density can be made.

The dipole intensity of a trap also depends on the geometry of the pixel and electrodes, the position of the trap in the pixel, the signal size, the clocking scheme used, etc, all things that can be simulated with C3TM. Using C3TM it is therefore possible to make a map of the dipoles produced by traps depending on their position in the pixel. To do this traps with a known τ_e value at a range of sub pixel positions are put in a single line of pixels with equidistant pixel positions. This means the traps, all with the same τ_e value, will have sub-pixels positions spread evenly over the pixel. A trap pumping scheme is then simulated for this line for a range of t_{ph} values, creating dipole curves for each trap.

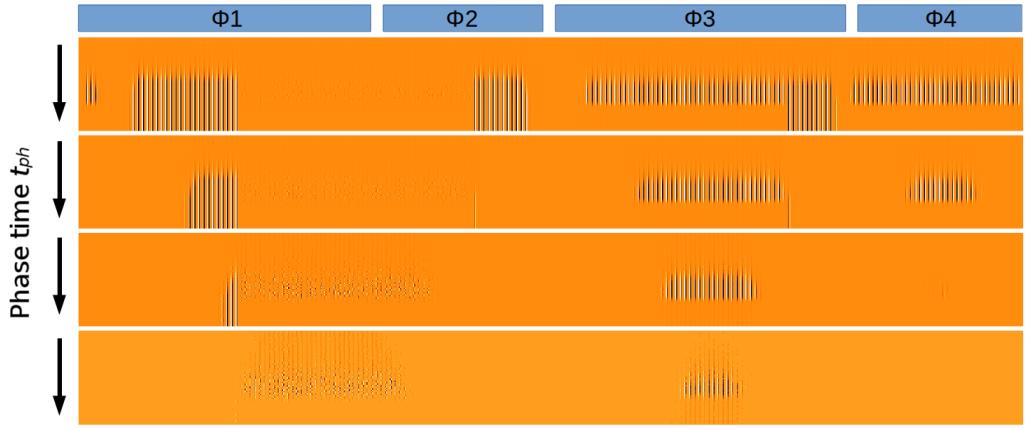

Figure 5. Trap pumping dipole map, showing the dipoles curves created by a range of phase times t_{ph} (in the vertical direction) and at different positions in the pixels, as mapped by the phases in the top of the figure. The four panels shows four different signal levels (from to to bottom) 100,000e$^-$, 10,000e$^-$, 1,000e$^-$, and 100e$^-$. Figure from Ref. 28.

An example of this is given in Fig. 5, where the pseudo-three phase clocking scheme has been simulated using the Euclid VIS CCD273 pixels. The CCD273 is a four-phase device, and the pseudo-three-phase clocking scheme couples two phases together, such that the charge is clocked between phases 12-3-4-1′2′-4-3-12, where 1′2′ denotes phases 1 and 2 in the adjacent pixel. The direction of the dipoles show which in which direction the charge will be moved and from the shape of the dipole curves it can be determined which equation should be used to extract the correct τ_e value of the traps (see also Ref. 28). Fig. 5 also shows how the shape and size of the charge cloud changes with signal size and what influence this has on the trap pumping data.

3.2 Interphase trapping

Based on the results from Fig. 5 it was initially believed that the pseudo-three-phase clocking scheme was the optimal clocking scheme for the Euclid VIS irradiation damage study. Experimental trap pumping data using this scheme was therefore obtained, but this data did not match the initial theoretical predictions or the initial simulated data.

An example of this is given in the Fig. 6 where the upper panel left shows a histogram of the fitted τ_e values from trap pumping data taken with the CCD273 at a temperature of 153 K. The upper right panel shows the same τ_e values plotted against their respective capture efficiency P_c. It was commonly assumed that trapping only occurs when the charge sits under the phase during the t_{ph} time, because the signal charge moves so fast from one electrode to the next during transfer, and with a low density over the interphase spacing, that no charge will be trapped in this transition. The middle panels of Fig. 6 shows the result of a simulation based on this assumption, i.e where the same trap pumping scheme has been simulated with no transition phases.

However, it was very clear that the simulated data did not match the experimental data very well, and a thorough analysis of this issue was therefore undertaken. During this analysis it became clear that the best explanation for this difference was indeed that a non-negligible amount of trapping actually can occur in even a very short transition phase. By adding in a 100 ns transition phase between each phase step in the simulation, the result shown in the lower panels of Fig. 6 was obtained. This result is clearly in much better agreement with the experimental data, and presents a very strong case for the existence of inter-phase trapping (for more detail see Ref. 28).

This result has implications not only for trap pumping theory, but also for how a radiation damaged CCD is operated in the most optimal way due to the physical nature of the simulation operation. It thus shows how C3TM can be used to test assumptions on device performance and improve our knowledge on radiation induced defects in CCDs.

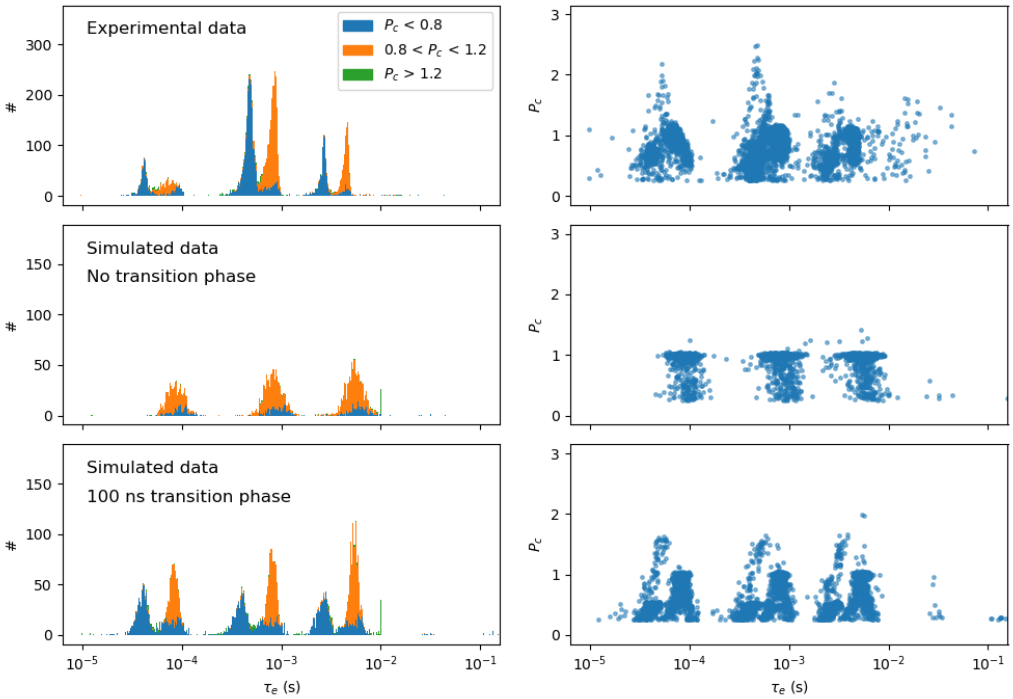

Figure 6. Trap pumping results from the Euclid radiation damage study. The panels on the left-hand side are histograms of the fitted τ_e-values and the panels on the right-hand side are the same τ_e values plotted against their respective capture efficiency P_c. *Upper panels:* Laboratory data taken with a un-irradiated CCD273 device at 153K. The data is from a single 2kx2k node clocked with the pseudo-three-phase clocking scheme. *Middle panels:* Simulation of the same situation, under the assumption that no inter-phase trapping will occur. *Lower panels:* Same as the middle panels, but using a 100 ns transition period between each phase step.

Based on these findings an alternative trap pumping scheme, the sub-pixel pumping scheme, was chosen for the Euclid VIS instrument and this scheme has now been implemented as part of the in-orbit calibration routines for the mission.[23]

3.3 Fitting charge tails

A common way of extracting the emission time constants of traps in a CCD is to fit the Extended Pixel Edge Response (EPER) tail[9] (or charge tail), with a sum of exponentials. However, this method can be problematic for two main reasons. The first is that fitting a curve with multiple exponentials can give a very broad range of results unless very narrow bounds on the fitting parameters are applied.

The second reason is the effect of recapture in the charge tail. An assumption that is usually made when fitting charge tails is that only charge captured in the illuminated region will be emitted in the tail. This means that charge captured within the tail itself is not taken into account. However, as shown in Fig. 7 then recapture has a significant effect on the slope of the tail and therefore has to be considered in order to get precise results.

Using C3TM these two issues can be addressed. As an example, laboratory data from the Euclid CCD273 radiation damage testing campaign is used.[29] Because the CCD273 has four readout nodes it was possible to irradiate each node differently. The irradiated devices therefore have information about three different fluence levels (as one node is used for comparison with other devices). The upper panel of Fig. 8 shows the charge tails from the lowest of the three irradiation levels, at four different signal levels. The experimental data is obtained at 12 different signal levels from ∼100 e^- to ∼100,000 e^-, but in order to not clutter the plot, only four signal levels is shown.

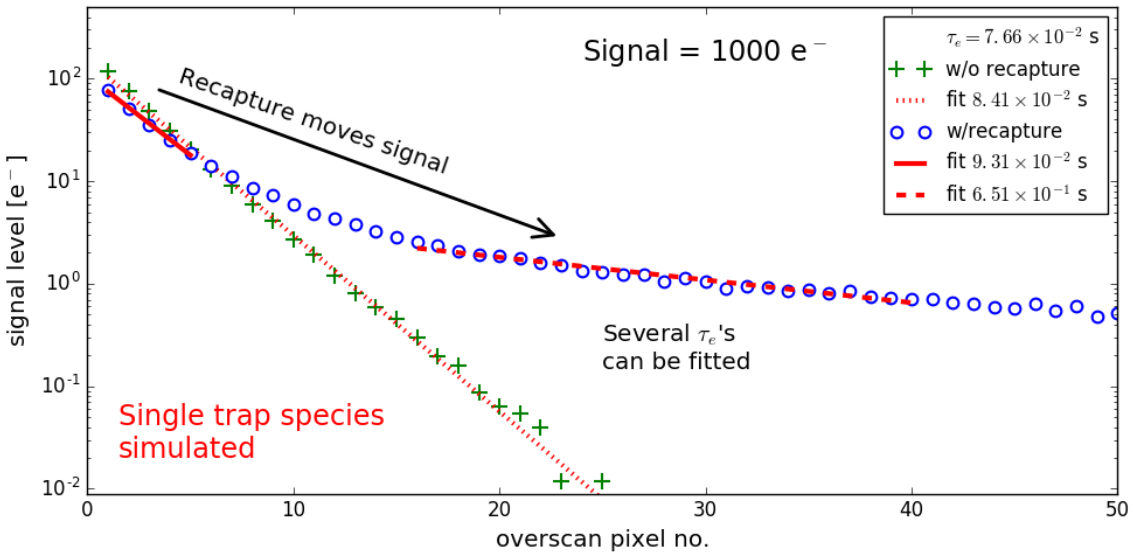

Figure 7. Charge tails from simulations of a single trap species with emission time constant of $\tau_e = 7.66 \times 10^{-2}$ s with and without recapture possible. A single exponential function are fitted to the charge tails to show that a single τ_e can be fitted very close to the real τ_e when recapture is not possible, while several τ_e's can be fitted in different regions, when recapture is possible. Figure from Ref. 1.

Table 1. Details of trap species used in the CCD273 charge tail simulation

name	τ_e (s)	E (eV)	σ_e (cm^2)	σ_c (cm^2)
(V-V)$^{--}$	8.0	0.41 ± 0.003	2e-15	1e-17
Unknown	1.59	0.34 ± 0.003	5e-16	1e-17
Continuum	7.87×10^{-2}	0.27 ± 0.05	5e-16	1e-17

By analysing the trap pumping data from the CCD273, the traps species most likely to influence the charge tails were identified. The analysis showed that besides the well-known species there was also the existence of a continuum of τ_e values as mentioned in Sect. 2.3. Using the trap species parameters detailed in Table 1 charge tails for each of the three species was simulated at a trap density of 10^{10} traps/cm^3. The simulation was run with operating parameters as close as possible to the ones used to create the experimental data and for the same 12 signal levels. These charge tails are shown in the lower panel of Fig. 8.

As the experimental data for each radiation level has been made with the same region of the device, it is safe to assume that the trap densities for each radiation level is the same. It is therefore possible to find the trap densities for the three species by fitting a combination of the three simulated charge tails to the experimental tail. As the trap density should scale linearly with the irradiation level of the device, it should also be possible to fit the three different irradiation levels with a simple constant. The best fit is therefore found by minimising the sum of the χ^2 over all 12 signal levels N_e for each radiation level K, such that the value to minimise is

$$\sum_K \sum_{N_e} \chi^2_{K,N_e} = \sum_K \sum_{N_e} \sum_{i=0}^{M-1} \frac{[D_{K,N_e}(x_i) - \Lambda_K S_{K,N_e}(x_i)]^2}{\sigma_{K,N_e}(x_i)^2} \,. \tag{8}$$

Here D is the experimental data, S is the simulated data, Λ is the constant associated with each radiation level, σ is the noise on the experimental data, and M is the number of data points in each tail.

The best fit is shown in Fig. 9. The charge tails seems to be fitting all signal levels and irradiation levels quite well. The 6×10^9 protons/cm^2 level has almost precisely 4 times the trap densities of the 1.5×10^9 protons/cm^2 level which matches the expected linear dependence with fluence level. The 3×10^9 protons/cm^2 level, however,

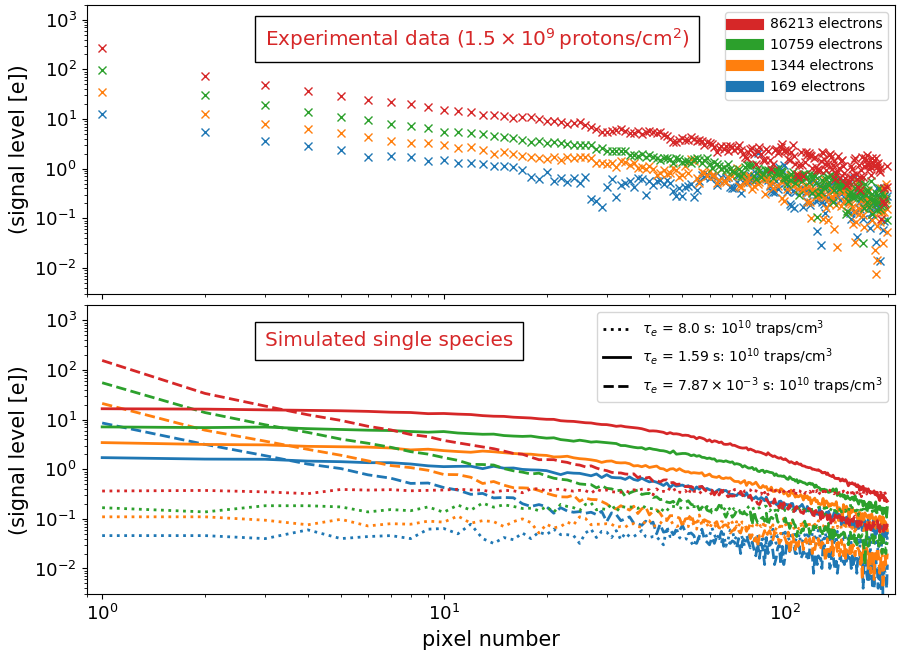

Figure 8. *Upper panel:* Experimental charge tails from the Euclid CCD273 radiation damage testing campaign at four different signal levels and at an irradiation level of 1.5×10^9 protons/cm^2. *Lower panel:* Simulated charge tails for three single species, all at a trap density of 10^{10} traps/cm^3.

has only 1.25 times the trap densities and does therefore not match the linear dependence. Other data from the CCD273 radiation damage study[29] show that the 3×10^9 protons/cm^2 level consistently gives lower than expected results and the C3TM simulation can therefore help prove that the node have not gotten the correct amount of radiation.

While this method is more precise than a simple fitting of a sum of exponentials, it can still only take recapture from the trap species that are being simulated into into account. To know how recapture from all three species affect the charge tails, a new simulation with the combined trap densities can be run for each signal and irradiation level. The result of this simulation is shown in Fig. 10, which shows that these charge tails fit the experimental data even better.

The results might be further improved by adjusting the trap parameters and rerunning the simulation. This can also help narrow down parameters, such as the emission and capture cross sections, that are difficult to estimate by other means. By including more signal levels and data made at different temperatures and with different clocking schemes etc., a much better understanding of the physical properties of the traps in the device can be gained. This knowledge will feed into the Euclid VIS radiation damage correction efforts to help improve the final data product.

4. CONCLUSIONS

The CEI CCD Charge Transfer Model (C3TM) for simulating charge transfer in a radiation damaged CCD is presented. C3TM is a Monte Carlo model that takes charge distribution simulations as a direct input. This is done to avoid making analytical assumptions on the size and density of the charge cloud, as this is shown to have a large effect on the the probability of capture and therefore also on the precision of the simulation.

A number of examples illustrating the performance of C3TM is given. Because C3TM runs on a sub-electrode level, it can be used to simulate the trap pumping technique, which can be used to extract information about the single defects in the silicon lattice. Comparing trap pumping data to simulations, evidence of inter-phase

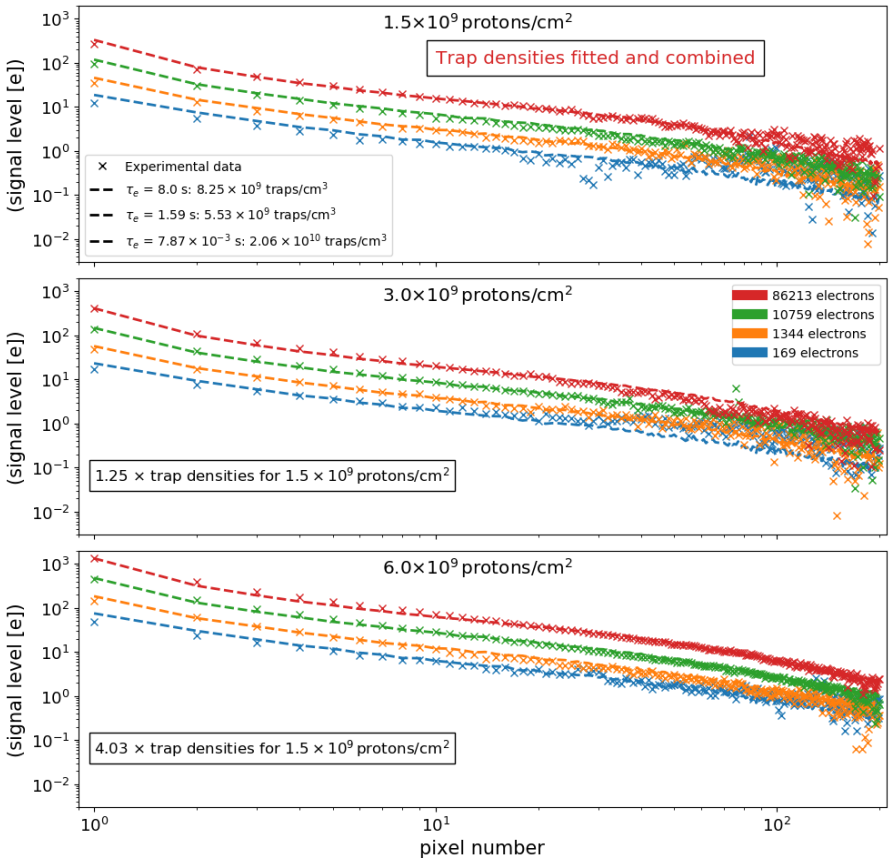

Figure 9. Trap densities of simulated single species fitted to experimental charge tails for three different irradiation levels. Even though the 3×10^9 protons/cm^2 level (middle panel) should have twice the amount of radiation than the top panel, the simulation shows that it has only 1.25 times the trap density. However, other data from the CCD273 radiation damage study show a similar result, which indicate that the node has not gotten the correct amount of radiation, an assumption that C3TM can help to prove.

trapping was found, thus showing how C3TM can be used to test assumptions on device performance and improve our knowledge on radiation induced defects in CCDs.

It is also shown how simulations of charge tails can be fitted to experimental data with very high precision, such that effects like recapture in the charge tail is included. C3TM can fit a range of signal and radiation levels with the same solution and without the use of additional analytical parameters or scaling. By using this method a much better understanding of the physical properties of the traps in the device can be gained.

As C3TM can help further our understanding of the properties of radiation induced defects, it can thus be an important tool for any space mission that depends on correcting the effects of radiation induced damage with very high precision.

REFERENCES

[1] Skottfelt, J., Hall, D. J., Gow, J. P. D., Murray, N. J., Holland, A. D., and Prod'homme, T., "Comparing simulations and test data of a radiation damaged charge-coupled device for the Euclid mission," *Journal of Astronomical Telescopes, Instruments, and Systems* **3**(2), 028001 (2017).

[2] Hall, D. J., Holland, A., Murray, N., Gow, J., and Clarke, A., "Modelling charge transfer in a radiation damaged charge coupled device for Euclid," in [*High Energy, Optical, and Infrared Detectors for Astronomy V*], *Proc. SPIE* **8453**, 845315 (July 2012).

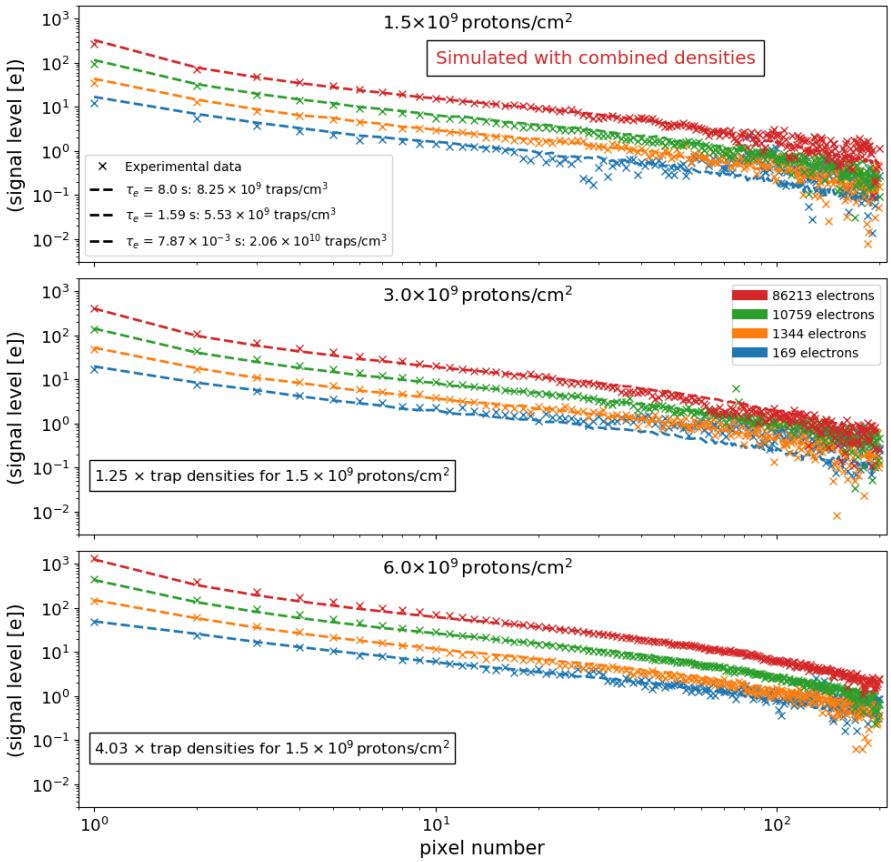

Figure 10. Simulation of combined species plotted along the experimental data using the trap densities found in Fig 9. The same solution is used for all signal and irradiation levels and no additional analytical parameters and scaling has been applied.

[3] Clarke, A. S., Hall, D. J., Holland, A., and Burt, D., "Modelling charge storage in Euclid CCD structures," *Journal of Instrumentation* **7**, C01058 (Jan. 2012).

[4] Hall, D. J., Gow, J., Murray, N. J., and Holland, A. D., "Optimization of device clocking schemes to minimize the effects of radiation damage in charge-coupled devices," *IEEE Transactions on Electron Devices* **59**, 10991106 (Apr 2012).

[5] Clarke, A., Hall, D., Murray, N., Gow, J., Holland, A., and Burt, D., "Pixel-level modelling and verification for the Euclid VIS CCD," in [*UV/Optical/IR Space Telescopes and Instruments: Innovative Technologies and Concepts VI*], *Proc. SPIE* **8860**, 88600V–88600V–12 (2013).

[6] Shockley, W. and Read, W. T., "Statistics of the Recombinations of Holes and Electrons," *Physical Review* **87**, 835–842 (Sept. 1952).

[7] Hall, R. N., "Electron-Hole Recombination in Germanium," *Physical Review* **87**, 387–387 (July 1952).

[8] Silvaco Inc, *ATLAS User Manual - Device simulation software* (September 2013).

[9] Janesick, J. R., [*Scientific charge-coupled devices*], SPIE-Intl Soc Optical Eng (2001).

[10] Kohley, R., Raison, F., and Martin-Fleitas, J. M., "Gaia: operational aspects and tests of Gaia Flight Model CCDs," in [*Astronomical and Space Optical Systems*], *Proc. SPIE* **7439**, 74390F (Aug. 2009).

[11] Mostek, N. J., Bebek, C. J., Karcher, A., Kolbe, W. F., Roe, N. A., and Thacker, J., "Charge trap identification for proton-irradiated p+ channel CCDs," in [*High Energy, Optical, and Infrared Detectors for Astronomy IV*], *Proc. SPIE* **7742**, 774216 (July 2010).

[12] Murray, N. J., Holland, A. D., Gow, J. P. D., Hall, D. J., Tutt, J. H., Burt, D., and Endicott, J., "Mitigating radiation-induced charge transfer inefficiency in full-frame CCD applications by 'pumping' traps," in [*High Energy, Optical, and Infrared Detectors for Astronomy V*], *Proc. SPIE* **8453**, 845317 (July 2012).

[13] Hall, D. J., Murray, N. J., Holland, A. D., Gow, J., Clarke, A., and Burt, D., "Determination of In Situ Trap Properties in CCDs Using a "Single-Trap Pumping" Technique," *IEEE Transactions on Nuclear Science* **61**, 1826–1833 (Aug. 2014).

[14] Murray, N. J., Burt, D., Hall, D. J., and Holland, A. D., "The relationship between pumped traps and signal loss in buried channel ccds," in [*UV/Optical/IR Space Telescopes and Instruments: Innovative Technologies and Concepts VI*], *Proc. SPIE* **8860** (2013).

[15] Cropper, M., Pottinger, S., Niemi, S., Azzollini, R., Denniston, J., Szafraniec, M., Awan, S., Mellier, Y., Berthe, M., Martignac, J., Cara, C., Di Giorgio, A.-M., Sciortino, A., Bozzo, E., Genolet, L., Cole, R., Philippon, A., Hailey, M., Hunt, T., Swindells, I., Holland, A., Gow, J., Murray, N., Hall, D., Skottfelt, J., Amiaux, J., Laureijs, R., Racca, G., Salvignol, J.-C., Short, A., Lorenzo Alvarez, J., Kitching, T., Hoekstra, H., Massey, R., and Israel, H., "Vis: the visible imager for euclid," *Proc. SPIE* **9904**, 99040Q–99040Q–16 (2016).

[16] Laureijs, R., Amiaux, J., Arduini, S., Augueres, J. ., Brinchmann, J., Cole, R., Cropper, M., Dabin, C., Duvet, L., Ealet, A., and et al., "Euclid Definition Study Report," *ArXiv e-prints* **1.1** (Oct. 2011).

[17] Hopkinson, G. R. and Mohammadzadeh, A., "Radiation effects in charge-coupled device (CCD) imagers and CMOS active pixel sensors," *International Journal of High Speed Electronics and Systems* **14**(02), 419–443 (2004).

[18] Lindegren, L., "Charge trapping effects in ccds for gaia astrometry," tech. rep., ESA (1998).

[19] Prod'homme, T., Brown, A. G. A., Lindegren, L., Short, A. D. T., and Brown, S. W., "Electrode level Monte Carlo model of radiation damage effects on astronomical CCDs," *MNRAS* **414**, 2215–2228 (July 2011).

[20] Massey, R., Stoughton, C., Leauthaud, A., Rhodes, J., Koekemoer, A., Ellis, R., and Shaghoulian, E., "Pixel-based correction for Charge Transfer Inefficiency in the Hubble Space Telescope Advanced Camera for Surveys," *MNRAS* **401**, 371–384 (Jan. 2010).

[21] Massey, R., Schrabback, T., Cordes, O., Marggraf, O., Israel, H., Miller, L., Hall, D., Cropper, M., Prod'homme, T., and Niemi, S.-M., "An improved model of charge transfer inefficiency and correction algorithm for the Hubble Space Telescope," *MNRAS* **439**, 887–907 (Mar. 2014).

[22] Short, A., Crowley, C., de Bruijne, J. H. J., and Prod'homme, T., "An analytical model of radiation-induced Charge Transfer Inefficiency for CCD detectors," *MNRAS* **430**, 3078–3085 (Apr. 2013).

[23] Skottfelt, J., Hall, D., Dryer, B., Bush, N., Campa, J., Gow, J., Holland, A., Jordan, D., and Burt, D., "Trap pumping schemes for the euclid ccd273 detector: characterisation of electrodes and defects," *Journal of Instrumentation* **12**(12), C12033 (2017).

[24] Wood, D., Hall, D. J., Murray, N. J., Gow, J. P. D., Holland, A., Turner, P., and Burt, D., "Studying charge-trapping defects within the silicon lattice of a p-channel ccd using a single-trap "pumping" technique," *Journal of Instrumentation* **9**(12), C12028 (2014).

[25] Wood, D., Hall, D., Gow, J. P. D., and Holland, A., "A study of the double-acceptor level of the silicon divacancy in a proton irradiated n-channel CCD," in [*High Energy, Optical, and Infrared Detectors for Astronomy VII*], *Proc. SPIE* **9915**, 99150J (Aug. 2016).

[26] Bush, N., Dryer, B., Lindley DeCaire, A., Burgon, R., and Holland, A., "A comparison of proton damage effects on P- and N-Channel CCDs I: Performance following cryogenic irradiation," in [*High Energy, Optical, and Infrared Detectors for Astronomy VIII*], *Proc. SPIE* **10709-23** (2018).

[27] FITS (Flexible Image Transport System), "https://fits.gsfc.nasa.gov/fits_home.html."

[28] Skottfelt, J., Hall, D. J., Dryer, B., Bush, N., Gow, J. P. D., and Holland, A. D., "Importance of charge capture in interphase regions during readout of charge-coupled devices," *Journal of Astronomical Telescopes, Instruments, and Systems* **4**, 018005 (Jan. 2018).

[29] Skottfelt, J., Dryer, B., Hall, D. J., Gow, J. P. D., and Holland, A. D., "Initial results from the Euclid VIS cryogenic irradiation campaign," in [*High Energy, Optical, and Infrared Detectors for Astronomy VIII*], *Proc. SPIE* **10709-98** (2018).